Indirect Electrothermal Acceleration of a Cold Gas Jet through Interaction of an arcjet Exhaust Flow for Space Propulsion Applications

IEPC-2019-A594

Presented at the 36th International Electric Propulsion Conference
University of Vienna • Vienna, Austria
September 15-20, 2019

Yuka Arai[1], Ryuta Futada[2], Yusuke Mizuno[3], Shun Takahashi[4], Kota Fukuda[5], and Hideyuki Horisawa[6]
Tokai University, Hiratsuka, Kanagawa, 2591292, Japan

and

Yu Sumoto[7]
Nippon Pneumatic MFG. Co., LTD, Nabari, Mie, 5180605

Abstract: In this study, numerical simulation on acceleration characteristics of a cold gas jet through utilization of an arcjet was conducted, where the supersonic free jet was accelerated through an interaction in a shear layer between the free jet and arcjet. In this analysis, the governing equations including two–dimensional compressible Reynolds–averaged Navier–Stokes equations (RANS) were calculated with a commercial code, ANSYS Fluent v.14.5. As for the turbulence model, a *k*–*ε* realizable turbulence model was employed. In this paper, when an arc flow is used for the center nozzle, the velocity is higher especially in potential core part than in the case of unheated flow because of a hot core flow of the arcjet.

Nomenclature

D,d	=	characteristic length
k	=	kinetic energy
M	=	Mach number
P	=	pressure
T	=	temperature
t	=	time
t^*	=	non–dimensional time
u	=	velocity
x	=	position
y	=	position
ε	=	turbulence disappearance rate
ρ	=	density

[1] Postgraduate student, Department of Mechanical Engineering, and ready.shb.omg@gmail.com.
[2] Undergraduate student, Department of Aeronautics and Astronautics, and gtee07k22@gmail.com.
[3] Postgraduate student, Department of Science and Engineering, and 7btad010@mail.u-tokai.ac.jp.
[4] Associate professor, Department of Prime Mover Engineering, and takahasi@tokai-u.jp.
[5] Associate professor, Department of Aeronautics and Astronautics, and fukuda@tokai-u.jp.
[6] Professor, Department of Aeronautics and Astronautics, and hideyuki.horisawa@gmail.com.
[7] Manager, Chemical Engineering Technical Section, and sumotoy@npk.co.jp.

Subscripts

0 = total
b = back

I. Introduction

THE current trend towards miniaturized satellites, which is not only mass limited but also power limited, has produced a strong interest in development of micropropulsion devices[1–4]. Although in the past, all of those miniaturized satellites have lacked propulsion systems altogether, future micro–spacecraft will require significant propulsion capability to provide a high degree of maneuverability and capability. The benefit of using electric propulsion for the reduction of spacecraft mass will likely be even more significant for mass limited micro-spacecraft missions.

Various potential micropropulsion systems for micro–spacecraft applications, such as ion thrusters, field emission thrusters, pulsed plasma thrusters (PPTs), resistojets, arcjets, etc., have been proposed and are under significant development for primary and attitude control applications. Arcjet thrusters are used for north–south station keeping of commercial geosynchronous satellites.[5,6] In this study, we investigated indirect aero–dynamical acceleration characteristics of a cold gas jet through an arcjet using numerical simulation.

II. Computational Method

In this study, a commercial CFD solver, ANSYS Fluent v.14.5, was employed to analyze an axisymmetric Reynolds–averaged Navier–Stokes equations. As for the turbulent model, realizable k–ε model[7] was employed. The fourth–order Runge–Kutta method and Roe–FDS method were employed for time– and spatial– discretization scheme, respectively.

A simulation model is illustrated in Fig.1 showing axisymmetric, coaxial, circular, triple nozzle jets. Dimensions of the axisymmetric domain are 150 mm and 20 mm in axial (x–direction) and radial (y–direction) directions, respectively. At an inlet boundary (left, at – x) on the centerline, three inlets of coaxial supersonic jets from a coaxial triple nozzle are placed. The right (at + x) and top (at + y) outer boundaries are outlet boundaries, and an axisymmetric boundary for the centerline (at y = 0).

A schematic illustration of the axisymmetric, coaxial, triple supersonic jets are shown in Fig.2. A diameter of the arcjet (nozzle 1) labeled as "D" is assumed as a characteristic length of the domain. The width of the smallest grid is 0.05 mm. The main flow subjected to the acceleration with a r c jet (nozzle 1) is a supersonic jet exhausted from nozzle 2. A jet from the third nozzle (nozzle 3) is an assisting jet for the supersonic jet from nozzle 2.

Outlet conditions are given in Table 1. Flows inside and outside of the nozzles are regarded as non–reactive air flows, and a arcjet is assumed as a high–temperature (or heated) non–reactive air jet, for simplicity.

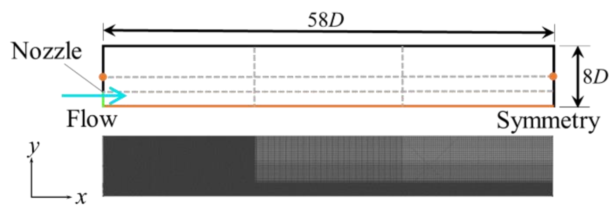

Figure 1. Simulation model.

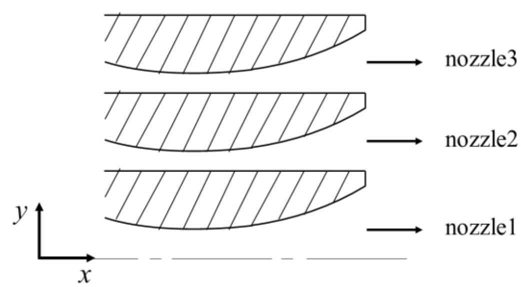

Figure 2. Schematic illustration of the axisymmetric, coaxial, triple supersonic jets.

Table 1. Outlet conditions of the simulation model.

Mach	T_0 [K]	P_b [Pa]
0	300	101325

III. Results and Discussions

A. The effectiveness of an arcjet on acceleration of a coaxial free jet

In this section, an investigation is conducted to assess the effectiveness of a arcjet on acceleration of a coaxial free jet. A simulation model and outer boundary are as described in Chap. Ⅱ.

An investigation is conducted on the influence of conditions of the arcjet (nozzle 1) on acceleration of a coaxial supersonic free jet. The conditions of the nozzles are listed in Table 2, where heated arcjet of nozzle 1 labeled as case1–1, and non–heated jet of nozzle 1 as case1–2.

Table 2. Numerical condition of case 1.

		Mach number	T_0 K	d_{throat} mm	$\dot{m}$ slm
nozzle 1					
case1–1	Heated	2.65	2000	1.5	24
case1–2	Non–heated	2.65	300	1.5	24
nozzle 2, nozzle 3					
nozzle 2	Non–heated	2	300	0.65	308
nozzle 3	Non–heated	1.7	300	0.20	152

Figure 3 shows the distributions of velocity magnitude of flow at non–dimensional time at t^* = 767 in case1–1 and case1–2, respectively. The contour of upper side shows the full of computational region and the bottom side shows the local from the nozzle exhaust. Since the total temperature of heated flow is much higher than that of non–heated flow (approximately 7 times), causing much difference in internal energy, higher velocities can be maintained to the downstream than non–heated flow. From fig.4, as for pressure, higher numbers can be maintained at downflow in non–heated jet condition (case1–2). In both cases normal shock waves at the nozzle 1 can be seen in the exhaust region. Oscillation of pressure distribution is occurring in x–axis direction in the nozzle exhaust region. As exhaust pressure is lower than atmospheric pressure, an overexpanded exhaust jet is observed at downstream region. In fig. 5, we visualized velocity magnitude and kinetic energy, which are normalized with the results of case1–2 (non–heated flow case) at x = 0.100 m from nozzle exhaust. It shows the normalized velocity and

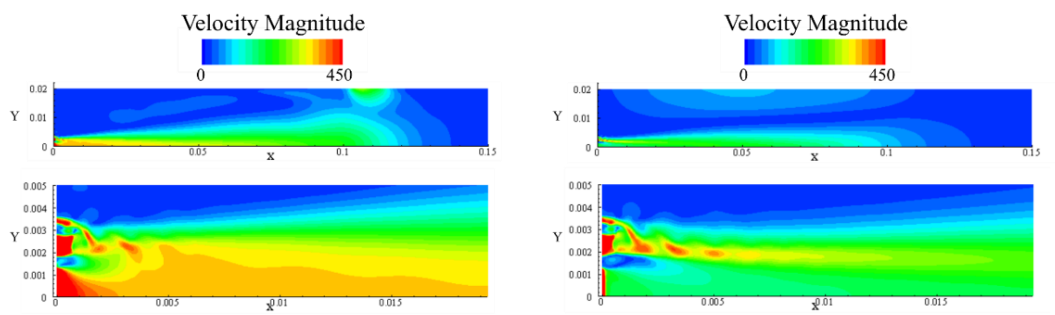

(a) case1–1 (Heated flow) (b) case1–2 (Non–heated flow)

Figure 3. Instantaneous flow distributions of velocity magnitude at non–dimensional time t^* = 767. The full (upper side) and local (bottom side) computational regions in (a) case 1–1 and (b) 1–2, respectively.

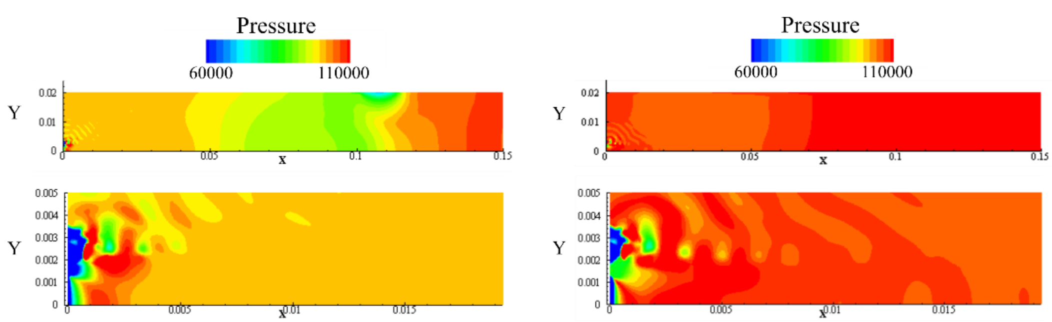

(a) case1–1 (Heated flow) (b) case1–2 (Non–heated flow)

Figure 4. Instantaneous flow distributions of pressure at non–dimensional time t^* = 767. The full (upper side) and local (bottom side) computational regions in (a) case 1–1 and (b) 1–2, respectively.

kinetic energy of case1–1 (heated flow case) is approximately 3.5– and 6–times higher than that of case1–2 near the center region respectively, especially at y/D = 4.5, a corresponding outer jet boundary, these of case 1 results 5– and 14–times higher level than case 2, respectively. From the results, we expected the jet augmentation of cold gas flow using heated supersonic jet is valid.

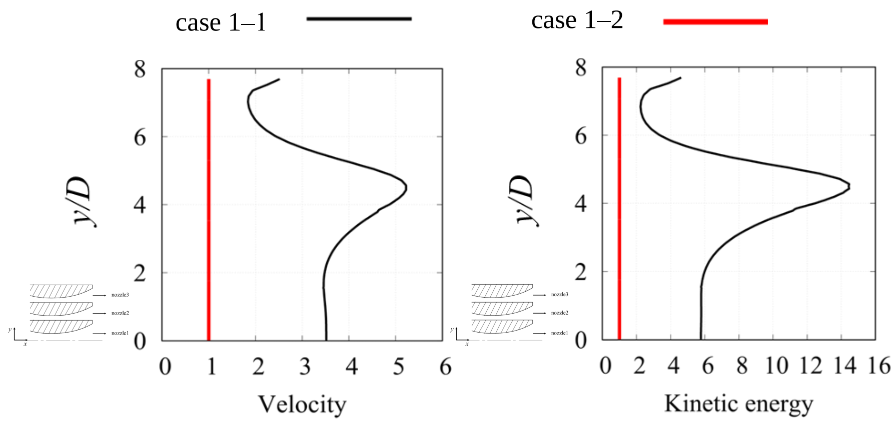

Figure 5. Graphs of normalized velocity magnitude and kinetic energy at *x* = 0.100 m from the nozzle exits.

In addition, gradients of axial (*x*–) component velocity in radial (*y*–) direction, *du/dy*, are considered. Figure 6 shows variations of the velocity gradients for heated and non–heated jet cases at *x* = 0.050 m downstream from the nozzle. With the heated jet case, magnitudes of the velocity gradients become largest at *y* = 0 to 0.002 m, corresponding to a separation between a central heated jet (nozzle 1) and a coaxial outer jet (nozzle 2), or namely at a shear layer. Moreover, at *y* = 0.003 to 0.004 m, corresponding to another separation, or shear layer, between nozzle 2 and nozzle 3, the values are large. On the other hand, in the non–heated jet case, tendencies are similar, however, their magnitudes are smaller than heated jet case.

Since local shear stresses acting on fluid elements are proportional to the local velocity gradients (d*u*/d*y*), momentum and energy transfers in the shear layer from an inner heated jet to an outer jet in the heated jet case must be more efficient than those of non–heated case. Moreover, higher magnitudes of the velocity gradients must be more efficient in the momentum and energy transfers.

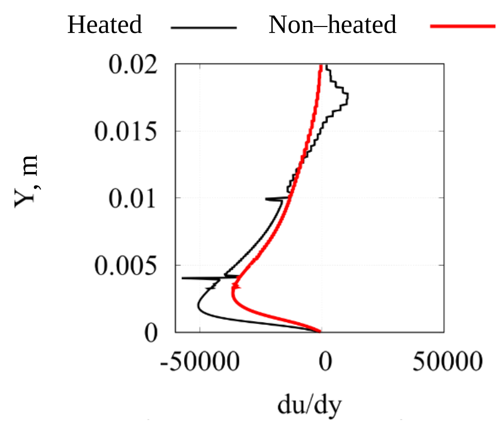

Figure 6. Variations of the velocity gradients for heated and non–heated jet cases at *x* = 0.050 m downstream from the nozzle.

B. The influence of total temperatures of the arcjet (nozzle 1) on acceleration of a coaxial supersonic free jet

In this section, the influence of total temperatures of the arcjet (nozzle 1) on acceleration of a coaxial supersonic free jet is compared and discussed. A simulation domain and dimensions are similar to those employed and described in the previous section. The conditions of the central arcjet are listed in Table 3, where different total temperatures of the heated arcjet of nozzle 1 are labeled as case2–1 for T_0 = 1000 K, case2–2 for T_0 = 3000 K, and case2–3 for T_0 = 4000 K.

Distributions of velocity magnitude and pressure in the nearfield region of the nozzles at non–dimensional time of t^* = 767 are shown in Figs.7 and 8, respectively. From the figure, it is shown that higher velocities can be maintained further to downstream region in higher temperature cases of heated jet conditions.

On the other hand, as for pressure distributions, higher values can be maintained to downstream region in lower temperature cases. In a case of the highest total temperature (case2–3), the largest values in magnitude of velocities can be maintained further to downstream region. As can be seen in these figures, since positions and strengths of normal or oblique shock waves in exhaust region of the heated jet outlet are different with the increase of total temperature, influences of the shocks on the downstream flow are significantly different. In these figures, pressure is significantly increased due to a Mach shock disk at the nozzle exhaust region, indicating a significant drop in Mach number is occurring except case2–3 where oblique shocks are dominant.

Distributions of normalized velocity and kinetic energy are plotted in Fig.9, which are normalized by the results of heated jet case (case1–1, T_0 = 2000 K) at x = 0.100 m downstream from the nozzle. From the figure, it is shown that magnitudes of the normalized velocities become larger with the increase of total temperatures. This is simply due to the larger total enthalpies with higher temperature cases. Although differences of the normalized kinetic energies for total temperatures of 1000 K, 2000 K and 3000 K are insignificant, significantly larger energies can be obtained with that of 4000 K by factor of 1.5. Due to smaller kinetic energies of the lower temperature cases at outer jet boundary, at y/d = 6, at downstream region, effects of the total temperature on increase of kinetic energies are significantly enhanced by factor of 1.7.

Table 3. Numerical condition of case 2.

nozzle 1

		Mach number	T_0 K	d_{throat} mm	$\dot{m}$ slm
case1–1	Heated	2.65	2000	1.5	24
case2–1			1000		
case2–2	Heated	2.65	3000	1.5	24
case2–3			4000		

nozzle 2, nozzle 3

		Mach number	T_0 K	d_{throat} mm	$\dot{m}$ slm
nozzle 2	Non–heated	2	300	0.65	308
nozzle 3	Non–heated	1.7	300	0.20	152

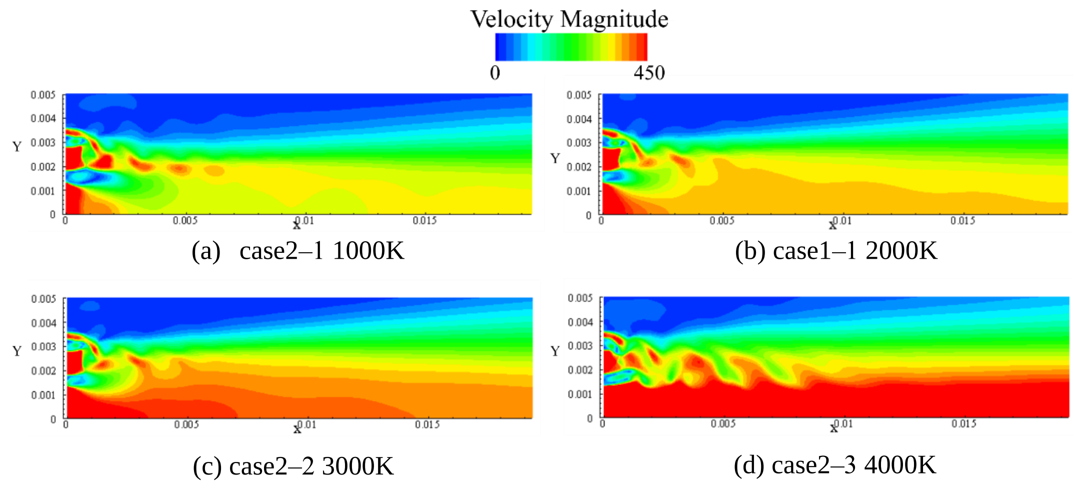

Figure 7. Instantaneous flow distributions of velocity magnitude at non–dimensional time t^* = 767. The local (bottom side) computational regions in case 1–1 and 2–1 to 2–3, respectively.

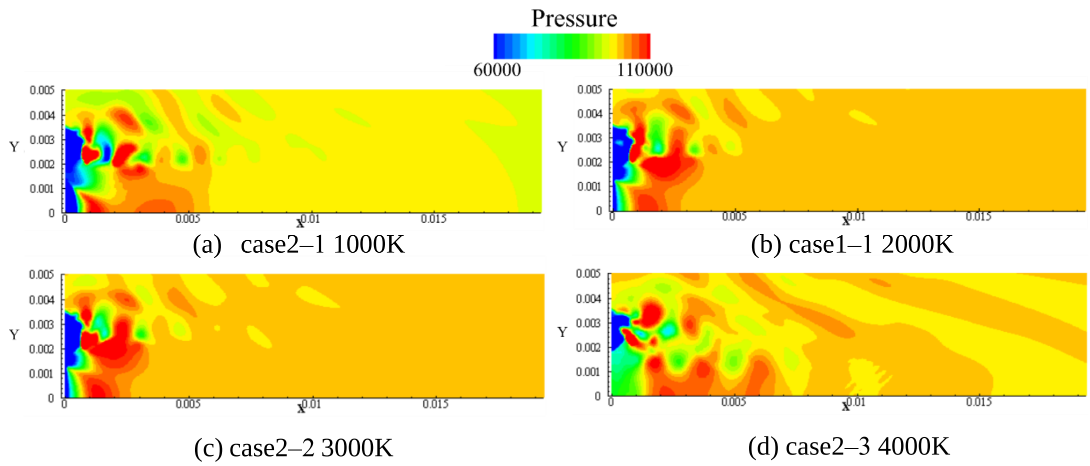

Figure 8. Instantaneous flow distributions of pressure at non–dimensional time t^* = 767. The local (bottom side) computational regions in case 1–1 and 2–1 to 2–3, respectively.

From the results, it can be expected that further increase of the total temperature is more effective in acceleration of coaxial outer jets.

Comparing results of total temperatures of 2000 K (case1–1) and 4000 K (case2–3), although the total enthalpy is increased by factor of 2, the gain of the kinetic energy is by factor of 1.5. Therefore, it appears that conversion efficiencies of the total enthalpies to kinetic energies are becoming suppressed with the increase of the total temperature due to the enhanced complexity of the flow.

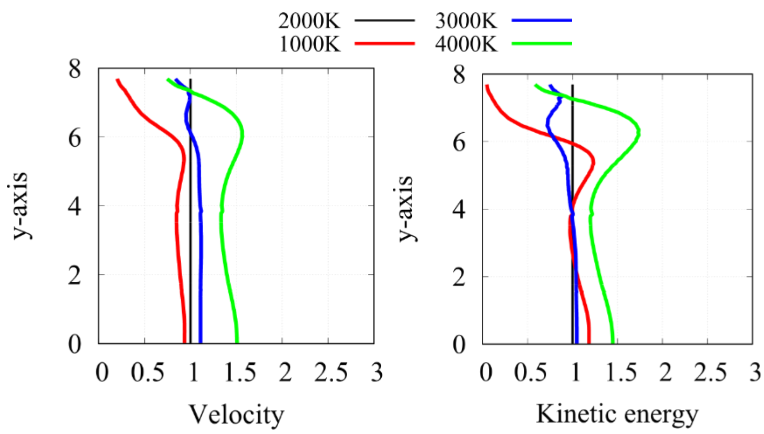

Figure 9. Distributions of normalized velocity and kinetic energy normalized by the results of the temperature of 2000 K case (case1–1) at x = 0.100 m downstream from the nozzle.

Variations of velocity gradients (du/dy) are plotted in Fig.10 for various total temperature cases at x = 0.050 m downstream from the nozzle. From the figure, it is shown, in all cases, that magnitudes of the velocity gradients become largest at y = 0 to 0.002 m, corresponding to a boundary between a central heated jet (nozzle 1) and a coaxial outer jet (nozzle 2), or namely at a shear layer. Moreover, relatively large velocity gradients are given at y = 0.003 to 0.004 m, corresponding to another boundary, or shear layer, between nozzle 2 and nozzle 3. In addition, the magnitudes of the velocity gradients become greater with the increase of total temperatures. Since local shear stresses acting on fluid elements depend on local velocity gradients (du/dy), it is shown that momentum and energy transfers in the shear layer from an inner heated jet to an outer jet become more effective with elevated temperatures. Larger magnitudes of the velocity gradients must be more efficient in the momentum and energy transfers, or namely acceleration of the flow.

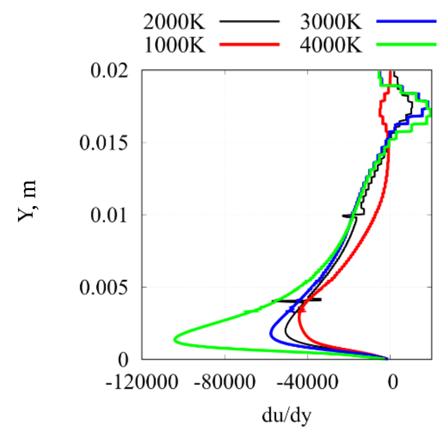

Figure 10. Variations of the velocity gradients for different cases of temperature of nozzle 1 at x = 0.050 m downstream from the nozzle.

C. The characteristics of a supersonic jet at low pressure environment

In this section, the influence of back pressure on acceleration of a coaxial supersonic free jet is assessed. A simulation domain and dimensions are similar to those employed and described in the previous sections. The conditions of the jet nozzles and back pressures are listed in Table 4, where different back pressures are labeled as case3–1 for P_b = 5000 Pa, case3–2 for P_b = 10000 Pa, and case1–1 for P_b = 101325 Pa as the reference.

Table 4. Numerical condition of case 3.

	Mach			T_0[K]			P_b[Pa]
	nozzle1	nozzle2	nozzle3	nozzle1	nozzle2	nozzle3	
case1–1	2.65	2	1.7	2000	300	300	101325
case3–1	2.65	2	1.7	2000	300	300	5000
case3–2							10000

Distributions of velocity magnitude and pressure in the low pressure at non–dimensional time of t^* = 767 are shown in Figs.11 and 12. From the figure, it is shown that oblique shocks and expansion fans are occurring and forming shock cell structures.[8] These are probably due to the higher static pressure than downstream region, where an underexpanded jet condition is established. It can be seen that the flows of both case are extended significantly and higher velocity magnitude can be maintained than that of case1–1. Since pressure distributions show jet shocks, reflection shocks, and jet boundaries at near exhaust region, it also can be seen that shock cells are produced by supersonic jets. Moreover, comparing distributions in these figures, it can be seen that lower the back pressure, the wider jet flow spreading in the axial direction and longer the cell lengths. This is considered to be because of the velocity increase with the decrease of local static pressures, where the flow is accelerated with greater energies in

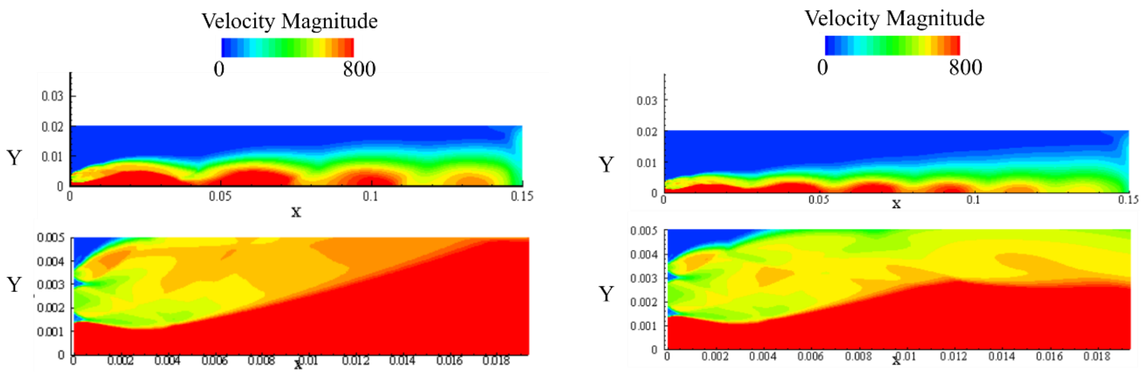

(a) case3–1 (P_b = 5000 Pa) (b) case3–2 (P_b = 10000 Pa)

Figure 11. Instantaneous flow distributions of velocity magnitude at non–dimensional time t^* = 767. The full (upper side) and local (bottom side) computational regions in (a) case 3–1 and (b) 3–2, respectively.

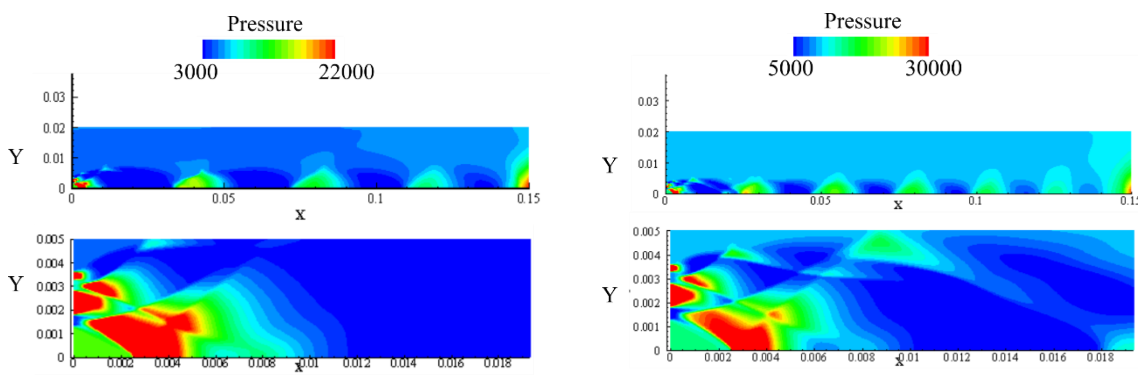

(a) case3–1 (P_b = 5000 Pa) (b) case3–2 (P_b = 10000 Pa)

Figure 12. Instantaneous flow distributions of pressure at non–dimensional time t^* = 767. The full (upper side) and local (bottom side) computational regions in (a) case 3–1 and (b) 3–2, respectively.

axial direction. There are little differences of locations and angles of expansion waves or compression waves established at near exit region. However, significant differences in cell lengths appear in downstream region.

Distributions of normalized velocity and kinetic energy are shown in Fig.13, which are normalized by the results of atmospheric pressure case (case1–1, P_b = 101325 Pa) at x = 0.100 m downstream from the nozzle. From the figure, it is shown that magnitudes of the normalized velocities and kinetic energies are relatively large at near centerline region except case3–1.

Moreover, comparing the results with case1–1, smaller back pressure cases (case3–1 and 3–2) show larger energy at near center region. However, at near outer jet boundary, the velocity magnitude and kinetic energy of case3–1 and 3–2 are lower than those of standard case.

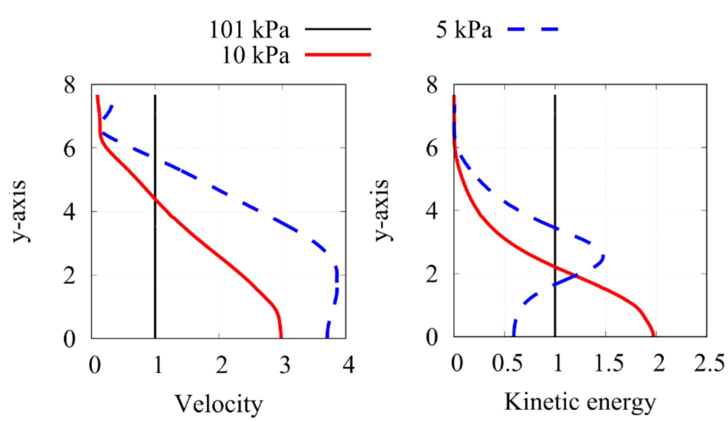

Figure 13. Distributions of normalized velocity and kinetic energy normalized by the results of the temperature of 101kPa case (case1–1) at x = 0.100 m downstream from the nozzle.

Variations of velocity gradients (d*u*/d*y*) are shown in Fig.14 for atmospheric pressure (case1–1) and lower pressure (case3–1 and 3–2) cases in back pressures at x = 0.050 m downstream from the nozzle. From the figure, it is shown that magnitudes of the velocity gradients of case3–1 become largest at y = 0.007 m, and those of case3–2 become largest at y = 0.005 m, corresponding to outer jet boundaries, or namely at shear layers. On the other hand, those of case1–1 show largest number at y = 0.002 m. From the results, it is shown that the locations of the maximum magnitudes are changing with back pressure.

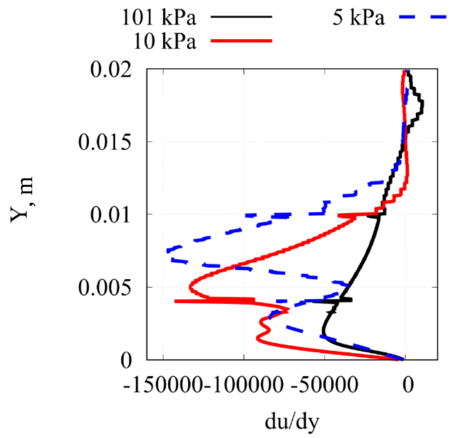

Figure 14. Variations of the velocity gradients for different cases of back pressure of nozzle 1 at *x* = 0.050 m downstream from the nozzle.

IV. Conclusion

In this study, numerical simulation on acceleration characteristics of a cold gas jet through interaction of an arcjet exhaust flow for space propulsion applications was conducted, where the supersonic free jet was accelerated through an interaction in a shear layer between the free jet and heated jet. All in the results obtained;

1. Momentum and energy transfers in the shear layer in the heated jet case must be more efficient than those of non–heated case.
2. Further increase of the total temperature of the arcjet was more effective in acceleration of coaxial outer jets.
3. Lower back pressure showed more effective in acceleration of the jets. The maximum values are transitioning with magnitudes of back pressure.

References

Periodicals

[1] Birkan, M. A., "Arcjet and Arc Heaters: An Overview of Research Status and Needs," Journal of Propulsion and Power, 12 (6), pp. 1011–1017, 1996.

[2] Butler, G. W., and Cassady, R. J., "Directions for Arcjet Technology Development," Journal of Propulsion and power, 12 (6), pp. 1026–1034, 1996.

[3] Auwerter–Kurtz, M., Glocker, B., Golz, T., Kurtz, H.L., Masserschmid, E.W., Riehle, M., and Zube, D.M., "Arcjet Thruster Development," Journal of Propulsion and Power, 12 (6), pp.1077–1083, 1996.

[4] Martinez–Sanchez, M., and Pollard, J.E., "Spacecraft Electric propulsion-An Overview," Journal of Propulsion and Power, 14 (5), pp.688–699, 1998.

[5] Sankovic, J. M., and Jacobson, D. T., "Performance of a Miniaturized Arcjet," NASA Technical Memorandum 107062, AIAA–95–2822, 1995.

[6]Zube, D. M., and Fye, D., "Low Bus Voltage Hydrazine Arcjet System for Geostationary Sattelites," AIAA–98–3631, 1998.

[7]Brescianini C. P., "Modified k–epsilon Model for Compressible Shear Flows, AIAA, **30** (1992), pp. 2161–2163.

[8]Mehta, R. C., and Prasad J. K., "Estimation of Shock–cell Structure of Axisymmetric Supersonic Free Jets," Indian J. Engineering and Materials Sciences, **3** (1996), pp. 141–147.